AIMS Geosciences

AIMS Geosciences, 12(2): 540–569.
DOI: 10.3934/geosci.2026021
Received: 20 January 2026
Revised: 01 April 2026
Accepted: 23 April 2026
Published: 02 June 2026

https://www.aimspress.com/journal/geosciences

Research article

Adaptive self-aware joint inversion of multiphysics geophysical data for volcanic monitoring: A methodological study

Paolo Dell'Aversana*

Independent researcher

* **Correspondence:** Email: paolodellaversa2024@virgilio.it; Tel: +39-3400736394.

Abstract: Volcanic risk monitoring and assessment are fundamental components of geohazard management, especially in the context of densely inhabited and socio-economically vulnerable regions. Traditional surface-based monitoring techniques, while valuable, often fall short in detecting deep, subsurface processes that precede eruptive events, particularly in areas where social, infrastructural, and logistical constraints hinder the deployment of high-resolution seismic surveys. These limitations are especially critical in volcanic settings where communities are exposed to multiple layers of risk, not only from natural hazards but also from structural inequalities and uneven access to protective measures. To address these challenges, we introduce a novel framework based on Self-Aware Joint Inversion, an adaptive, learning-driven method for the integration of multi-physics geophysical data. By combining seismic and non-seismic geophysical approaches, such as electrical resistivity tomography, gravity, and electromagnetic methods, within a self-optimizing joint inversion technique, our approach enables the dynamic and high-resolution imaging of subsurface processes that are directly linked to magma and fluid migration. Unlike conventional models that often remain shallow or static, this methodology offers time-lapse capabilities and deeper investigation, thereby enabling early detection of phenomena critical to volcanic risk forecasting. The method was tested on synthetic case studies simulating realistic volcanic conditions, enabling rigorous evaluation of resolution, adaptability, and potential operational performance. Results indicated that this approach can reconstruct subsurface anomalies associated with pre-eruptive activity, even in scenarios where classical monitoring frameworks would fail. Beyond its scientific contribution, this methodology is explicitly designed to be non-invasive and scalable, making it particularly suitable for application in sensitive inhabited zones.

Keywords: volcanic hazard; geophysics; data integration; joint inversion; self-learning

1. Introduction

Volcanic risk monitoring and assessment aim to minimize the impact of volcanic activity on human life, infrastructure, and the environment [1–7]. Modern volcanic monitoring systems typically rely on a combination of geophysical, geochemical, remote sensing, and ground-based techniques, often supported by advanced data integration and modeling frameworks. Cigna et al. [8] provides a comprehensive overview of how modern remote sensing technologies are used to monitor volcanic activity and assess associated risks, highlighting the integration of different satellite sensors. Loughlin et al. [9] present a global assessment of volcanic hazards and risks, offering a systematic analysis of volcanic threats to society and the importance of international monitoring frameworks. Ebmeier et al. [10] synthesize global satellite data on volcanic deformation to analyze magmatic processes, discussing how space-based observations improve our understanding of magma storage and transport. Pyle et al. [11] introduce the integration of remote sensing observations with numerical modeling, emphasizing how combining these two approaches enhances the prediction and interpretation of volcanic phenomena. Francis [12] explores the early capabilities and future potential of satellite remote sensing for volcano monitoring, focusing on thermal and topographic data collection. Sansivero & Vilardo [13] describe the technical processing of long-term thermal infrared image series from ground-based networks, focusing on detection of thermal anomalies in volcanic areas. Laiolo et al. [14] demonstrate how combining satellite and ground-based geophysical data can track magma migration in real-time, using Mount Etna as a primary case study for shallow feeding systems.

More broadly, a fundamental principle underlying these approaches is the importance of multidisciplinary integration, which maximizes the informational value of different methodologies when they are properly combined. For example, Alperovich et al. [15] demonstrated that integrating ground-penetrating radar (GPR) and electrical resistivity tomography (ERT) within a unified analytical framework can significantly improve the reliability of subsurface interpretations compared with analyses based on a single method. The synergistic use of multiple geophysical datasets can therefore substantially increase confidence in subsurface characterization, particularly in complex geological settings.

Considerable attention has been given to the development of non-conventional approaches for the quantitative interpretation of geophysical data, complementing traditional deterministic inversion and forward modeling techniques. These approaches aim to address the inherent non-uniqueness and uncertainty that characterize geophysical inverse problems, as well as the limitations associated with interpreting individual datasets in isolation. Advanced signal-processing methods, multi-resolution analysis, and hybrid data-fusion strategies have been proposed to enhance the extraction of meaningful information from heterogeneous geophysical observations. Wavelet-based methods and multi-scale signal analysis have proven to be particularly effective in the detection and characterization of subsurface anomalies, enabling the identification of localized features within complex geophysical signals [16,17]. These approaches enable the decomposition of geophysical data into different spatial or temporal scales, thereby improving the interpretability of signals affected by noise or overlapping geological responses.

Another important class of non-conventional approaches involves probabilistic and stochastic inversion methods, which explicitly incorporate uncertainty into the interpretation process. Bayesian inversion frameworks, for example, enable the integration of prior geological information with geophysical observations, providing probabilistic estimates of subsurface parameters and helping to quantify the range of admissible models compatible with the data [18–20]. Such methodologies have become increasingly relevant in complex geological environments, where deterministic solutions may not adequately capture the variability and ambiguity inherent in the data.

Similarly, joint inversion and structurally coupled inversion techniques have emerged as powerful tools for the integrated interpretation of multiple geophysical datasets. Methods based on structural constraints, such as cross-gradient coupling, enable different physical datasets to be inverted simultaneously while preserving structural similarities between the resulting models [21–24]. These approaches can significantly improve the robustness and geological consistency of subsurface reconstructions compared with independent inversions.

Moreover, advances in computational capabilities have facilitated the application of machine learning and data-driven approaches to geophysical interpretation. Techniques such as neural networks, pattern recognition algorithms, and hybrid physics–data frameworks can identify complex relationships within large geophysical datasets and assist in the interpretation of multidimensional monitoring data [25–27]. Although still evolving, these methods offer promising perspectives for improving the efficiency and reliability of quantitative geophysical analysis.

Within this expanded perspective, the concept of integration extends beyond the purely technical domain. Volcanic risk analysis is not only a scientific and engineering task but also a societal instrument aimed at protecting vulnerable communities and strengthening resilience to natural hazards. In a world increasingly characterized by urban expansion and growing social inequality, volcanic hazard exposure intersects with complex socioeconomic realities, requiring integrated strategies that account for both physical threats and social vulnerability.

Over recent decades, scientific and technological progress has enhanced our ability to detect early warning signals of volcanic unrest, contributing to more informed decision-making and tailored risk mitigation strategies. However, this technical advancement must be contextualized within broader societal frameworks that include public policy, governance, access to resources, and the lived experiences of those most at risk. Traditional monitoring efforts, focused on seismicity, ground deformation, gas emissions, thermal anomalies, remote sensing, and hydrological variations, remain indispensable. Yet, in densely populated or socioeconomically disadvantaged areas, where vulnerability is compounded by limited infrastructure and institutional capacity, such surface-based methods may be insufficient to fully assess the depth and complexity of subsurface processes. Many of the most dangerous volcanic phenomena originate deep below the surface, eluding detection by conventional means and leaving at-risk communities with little time to respond. In response to these challenges, in this paper, we propose a novel geophysical monitoring framework based on self-aware, joint inversion of multidisciplinary datasets, a next-generation methodology that integrates high-resolution, time-lapse imaging with machine learning and adaptive optimization. This approach enhances the interpretability and resilience of monitoring systems, particularly in urbanized or socially complex volcanic regions where early warning is critical but technically and institutionally difficult to achieve. Beyond improving technical capacity, this integrated strategy aligns with inclusive disaster risk reduction (DRR) frameworks by promoting spatially and temporally aware hazard assessments

that can inform equitable, community-focused policies. It enables the detection and interpretation of dynamic subsurface changes, such as magma and fluid migration through fault networks, by leveraging seismic, electromagnetic, and gravimetric anomalies in real time. Such capabilities are indispensable for capturing early warning signs that may not manifest directly at the surface but have profound implications for nearby populations.

Before entering the technical discussion, it is important to clarify that the primary objective of this study is for methodological purposes. The framework presented here focuses on the development and testing of an adaptive self-aware joint inversion strategy designed to improve the integration and interpretation of multi-physics geophysical datasets. While the approach may have potential applications in volcanic risk monitoring and hazard assessment, we do not aim to directly address the broader socio-economic aspects of risk management. Instead, the purpose of the synthetic experiments presented in this paper is to evaluate the technical feasibility of the proposed inversion framework under controlled conditions. The reference to high volcanic risk in densely populated volcanic regions should therefore be understood primarily as a motivating context in which improved subsurface imaging capabilities, continuous multi-parameter monitoring, early warning systems, emergency planning, and effective communication strategies, are particularly valuable, rather than as a claim that methodological developments alone can resolve the complex societal and economic challenges associated with volcanic risk management.

In the following sections, we present the theoretical basis and implementation of this integrated geophysical approach, showing its value through synthetic case studies that simulate complex volcanic settings. These examples illustrate not only the method's scientific robustness but also its potential to support transdisciplinary risk governance, bridging the gap between geophysical data, social vulnerability indicators, and participatory risk management strategies.

2. Methodological principles

2.1. Adaptive multi-physics imaging in volcanic systems

Capturing critical volcanic processes, such as magma ascent, deep fluid migration, and pressure accumulation in magmatic or hydrothermal systems, requires geophysical imaging techniques capable of resolving subsurface properties evolving over short timescales (from hours to days). While full-resolution 3D seismic imaging remains the benchmark for detailed subsurface characterization, its repeated use in densely populated volcanic regions is often impractical. The high economic cost, social disruption, regulatory complexity, and potential risks to infrastructure make it unsuitable for frequent (time-lapse) surveys.

To address these limitations, we propose an innovative and pragmatic alternative: A high-resolution joint inversion of multidisciplinary non-seismic geophysical data, such as geoelectric, electromagnetic (e.g., magnetotelluric or CSEM), gravity, and gravity gradient measurements. These methods offer key advantages over seismic techniques for time-lapse volcanic monitoring, such as:

- Low environmental and social impact: They are non-invasive and cause minimal disturbance to local populations, making them ideal for repeated surveys in inhabited areas.
- Cost-effectiveness and logistical simplicity: These methods are significantly less expensive and easier to deploy than seismic campaigns, enabling more frequent acquisitions and better temporal resolution of subsurface changes. It must be emphasized that the availability, spatial

coverage, and temporal continuity of monitoring data depend on logistical, institutional, and economic factors that are outside the scope of this study. The methodology proposed in this work cannot replace the need for appropriate investments in monitoring infrastructures but rather aims to maximize the scientific value of the data that can realistically be acquired in each operational context.

- Complementarity with seismic constraints: When high-resolution seismic data (as well as borehole data) is available from dedicated campaigns, it can be used to construct a reliable geometrical framework (e.g., faults, fractures, and geological layering). This structural model can then be used as a geometrical constraint in the joint inversion of non-seismic data, thereby enhancing spatial resolution and interpretability of the inverted models.

To further improve the inversion results, we employ a novel approach called Self-Aware Joint Inversion [28]. This methodology introduces adaptive mechanisms that autonomously optimize key hyperparameters during the inversion process, including data weights, learning rates, and smoothing parameters, based on the system's internal recognition of uncertainties, conflicts, or instabilities. Unlike traditional joint inversion frameworks, which rely on static fusion rules and fixed optimization strategies, self-aware inversion adapts dynamically, prioritizing robust features and coherent anomalies.

This self-regulating behavior is particularly advantageous in volcanic settings, where small but meaningful geophysical signals (such as increased electrical conductivity or reduced density due to fluid or magma intrusion) can serve as precursors to eruptive events. By highlighting and reinforcing such critical features through learned importance, self-aware inversion enhances the sensitivity and reliability of early warning systems.

In summary, the proposed strategy, a time-lapse, self-aware, high-resolution, constrained joint inversion of low-impact geophysical data, provides an effective and sustainable tool for volcanic monitoring. It offers the dual benefit of minimizing disturbance to local communities and capturing high-resolution multi-physics models of the subsurface. When seismic or borehole data are available, they can serve as valuable constraints, further boosting the resolving power of non-seismic observations. This integrated and adaptive approach opens new avenues for safe, scalable, and insightful monitoring of volcanic systems, with benefits especially in densely populated areas.

2.2. Overview of joint inversion

Joint inversion in geophysics refers to the integrated interpretation of multiple datasets to generate a coherent and unified model of the subsurface [29–42]. Methodologies of data/model fusion have evolved from foundational, multi-domain integration of geophysical datasets [29,30,31,41] to complex, self-adaptive, and self-aware deep learning systems for enhanced analysis and interpretation of images in multiple domains [43,44]. Core research focuses on structural coupling for aquifer characterization, lithological classification, and subsurface imaging [32–38], alongside specialized workflows for reservoir and borehole data integration [39,40,42]. These advancements represent a shift toward integrating rock physics with sophisticated, AI-driven adaptive optimization techniques.

In this study, we discuss (through a sequence of demonstrative synthetic tests) joint inversion of seismic reflection, geoelectrical, and gravity data to achieve more accurate and geologically consistent estimations of subsurface properties. The core idea behind joint inversion lies in the complementarity of geophysical methods: Each data set is sensitive to different physical properties and combining multi-physics observations provides a more complete picture. These properties often exhibit spatial correlations, reflecting the presence of significant subsurface anomalies. For instance, seismic velocity mostly reflects mechanical and elastic characteristics such as stiffness, density, porosity, and lithology.

In contrast, electrical resistivity depends on factors like fluid content, salinity, porosity, mineralization, and pore connectivity. By jointly inverting seismic, electrical (or electromagnetic), and gravity data, we can better constrain the subsurface model and mitigate the ambiguity and non-uniqueness typical of single-method inversions.

The inversion workflow (illustrated in Figure 1) consists of the following core components:

- Forward Modeling: we simulate seismic, gravity, and electrical data based on initial subsurface models using proprietary modeling software. In this approach, seismic information helps define the major structural boundaries and geometrical features of the system, thereby improving the interpretability and stability of the joint inversion of the other geophysical parameters.
- Data Misfit Evaluation: Simulated data (predicted responses) are compared with actual measurements (observed responses), and a joint cost functional (Φ_{joint}) is computed.
- Iterative Model Updating: Model parameters are iteratively adjusted to minimize the total misfit (Φ_{mis}). This involves a weighted combination of the individual misfits from each dataset and may use gradient-based, stochastic, or hybrid optimization strategies.
- Structural and Petrophysical Constraints: Optional constraints, such as the cross-gradient term (Φ_X) or analytical rock physics relationships ($\Phi_{analytic}$), are incorporated to enhance structural and physical consistency between models.
- Regularization (Φ_{reg}): Additional prior constraints, such as spatial smoothness (e.g., via Tikhonov regularization), are applied to guide the inversion toward geologically plausible solutions.
- Each of these elements is weighted using user-defined coefficients (λ_i) that can be changed by the self-aware approach, without any human intervention, as explained below.

The framework adopted here draws from well-established approaches in literature. For example, Gallardo and Meju [21,22] introduced the widely used cross-gradient constraint; De Stefano et al. [41] detail the mathematical structure of each objective function term; and Dell'Aversana et al. [42] presented a stochastic joint inversion framework rooted in Bayesian theory and uncertainty quantification.

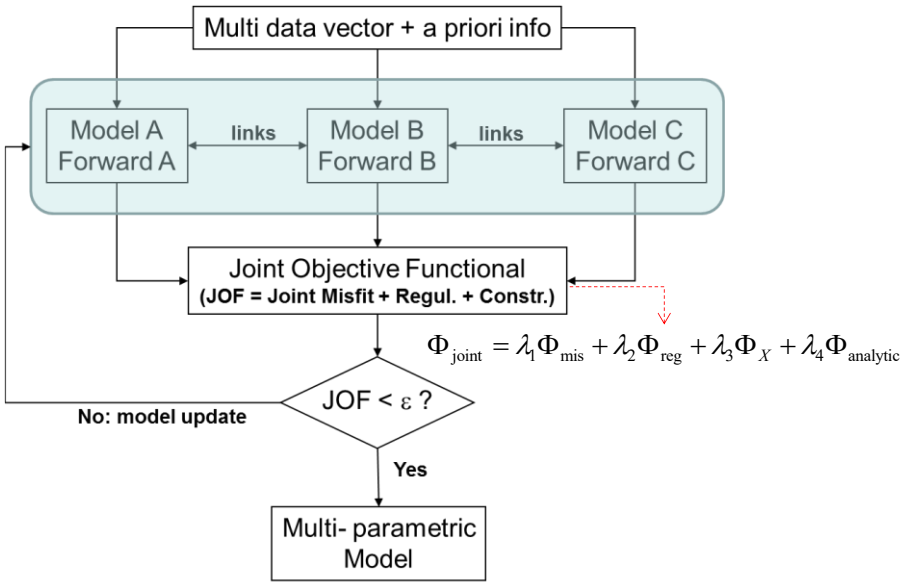

Figure 1. Major blocks of the joint inversion approach.

Let us summarize the mathematical framework of multi-physics joint inversion (additional details are provided in the Appendix). The global vector of unknown model parameters $\boldsymbol{m}$ in the model space $\boldsymbol{M}$ is defined as the concatenation of several parameter vectors associated with different physical domains:

$$\boldsymbol{m} = [\boldsymbol{m_1^T}, \boldsymbol{m_2^T}, \dots, \boldsymbol{m_k^T}]^T \quad (1)$$

where each subvector $\boldsymbol{m_i}$ represents the set of model parameters describing the subsurface properties in the *i-th* geophysical domain (e.g., seismic velocity, electrical resistivity, density, and magnetic susceptibility).

The state of information on the model parameters is described by the prior model $\boldsymbol{m_{prior}}$ and by $\boldsymbol{C}_M$, the model covariance matrix that accounts for the associated uncertainties.

Similarly, the global data vector $\boldsymbol{d}$ in the data space D is defined as the concatenation of the different datasets acquired by the geophysical methods:

$$\boldsymbol{d} = [\boldsymbol{d_1^T}, \boldsymbol{d_2^T}, \dots, \boldsymbol{d_k^T}]^T \quad (2)$$

where each subvector $\boldsymbol{d_i}$ contains the observations corresponding to the *i-th* physical experiment (e.g., seismic travel times, electric potentials, gravity anomalies, and electromagnetic responses).

The forward operator linking model parameters and data is therefore a composite operator composed of the forward operators associated with each geophysical method:

$$\boldsymbol{d} = \boldsymbol{g}(\boldsymbol{m}) = \begin{bmatrix} \boldsymbol{g_1}(\boldsymbol{m_1}) \\ \boldsymbol{g_2}(\boldsymbol{m_2}) \\ \vdots \\ \boldsymbol{g_k}(\boldsymbol{m_k}) \end{bmatrix} \quad (3)$$

where $\boldsymbol{g_i}$ represents the forward modeling operator for the *i-th* physical domain.

In the Bayesian framework [18,42] (one of the many possible optimization approaches usable for joint inversion of geophysical data), an iterative procedure linearizes the forward model around the current model $\boldsymbol{m}_{\mathrm{n}}$ and obtains a new model $\boldsymbol{m}_{\mathrm{n+1}}$ using the Jacobian matrix $\boldsymbol{J}_{\mathrm{n}}$ of the derivatives of the forward model equation with respect to the current model parameters:

$$\boldsymbol{m}_{n+1} = \boldsymbol{m}_n - \eta_n (\boldsymbol{J}_n^T \boldsymbol{C}_D^{-1} \boldsymbol{J}_n + \boldsymbol{C}_M^{-1})^{-1} \left[\boldsymbol{J}_n^T \boldsymbol{C}_D^{-1} (\boldsymbol{d}_n - \boldsymbol{d}_{obs}) + \boldsymbol{C}_M^{-1} \left(\boldsymbol{m}_n - \boldsymbol{m}_{prior}\right)\right], \quad (4)$$

where η_n is the learning rate and $\boldsymbol{C}_D$ is the covariance matrix that takes into account the uncertainties due to the measurements and the modeling. $\boldsymbol{C}_M$ is the covariance matrix that considers the uncertainties on model parameters.

At each iteration, the predicted data $\boldsymbol{d_n} = \boldsymbol{g}(\boldsymbol{m_n})$ are compared with the observed data $\boldsymbol{d}_{obs}$, and the solution is obtained by updating the current model until the posterior probability density of the model is maximized.

The posterior covariance matrix of the model space, $\boldsymbol{C}_{M,post}$, describes the uncertainty of the solution,

$$\boldsymbol{C}_{M,\,post} = (\boldsymbol{J}_n^T \boldsymbol{C}_d^{-1} \boldsymbol{J}_n + \boldsymbol{C}_M^{-1})^{-1}. \quad (5)$$

2.3. Self-aware joint inversion strategy

Our implementation builds on a Bayesian joint inversion method or, alternatively, on a robust gradient-based joint inversion algorithm, enhanced by self-aware hyperparameter tuning (see also Appendix for methodological and mathematical details). The objective is to simultaneously invert seismic, geoelectric, and/or gravity data to retrieve models of seismic velocity, electrical resistivity, and bulk density from data (reflection travel times, electric potentials, and Bouguer anomalies). The optimization strategy consists of the following key components:

(A) Bayesian Update or Gradient-Based Model Update

The algorithm predicts data from the current velocity and resistivity models, calculates the misfit with the observed data, and computes the gradient of the objective function. Model parameters are updated iteratively, reducing the mismatch and improving model accuracy.

(B) Cross-Gradient Coupling

A cross-gradient term encourages structural similarity between the multi-physics models. This term tends to zero when structural features (e.g., interfaces and faults) align in the domains. It penalizes structural misalignments, enforcing geological consistency even if the physical properties differ.

(C) Adaptive Model Smoothing

Gaussian smoothing is applied to all models to suppress noise and unrealistic artifacts. The smoothing strength is high in early iterations (to ensure stability) and progressively reduced to enable finer structural details to emerge later in the process.

(D) Self-Aware Hyperparameter Adjustment

A key innovation of the workflow is the dynamic, self-aware adjustment of hyperparameters, including learning rates, data weights, and smoothing factors. These hyperparameters are continuously adapted based on the behavior of the misfit functions. For example, if the misfit is decreasing steadily, the learning rate is optimally reduced (without any human intervention) to avoid overfitting; if convergence slows, the rate is increased to enhance efficiency. Additional details are discussed in the next subsection and in the Appendix.

(E) Iterative Inversion Loop

Starting from reasonable initial models (built based on all the available information), the algorithm simulates predicted responses using separate forward solvers for each domain. These models are updated iteratively using gradients, smoothing, and cross-gradient constraints.

2.4. Expected advantages

As outlined above, this approach integrates joint inversion with adaptive learning techniques that autonomously tune the learning rate and other hyperparameters during the inversion. Traditionally, parameters like the learning rate and the weights between the different data sets are fixed or manually adjusted. However, in challenging situations, such as volcanic scenarios, where models are highly complex, it is advantageous to tune these parameters dynamically. Our algorithm achieves this by continuously monitoring the evolution of the cost functions associated with seismic resistivity and density models. When misfits improve, learning rates are automatically increased to accelerate convergence. When misfits deteriorate, learning rates are reduced to prevent instability or overfitting. This strategy enables the algorithm to strike a dynamic balance between exploration (discovering new

solutions) and exploitation (refining existing ones). Similar adaptive strategies are applied to other hyperparameters as well.

The main benefit of this self-learning approach lies in its responsiveness to data behavior, enabling faster and more reliable convergence, especially when faced with incomplete or noisy datasets. Furthermore, it helps avoid local minima, a common pitfall in geophysical optimization.

In the next section, we present a series of synthetic tests that illustrate the ability of the self-aware joint inversion method to detect and characterize multi-physics anomalies, relevant to real-world situations in dynamic volcanic scenarios.

3. Simulations

3.1. Test 1. Detection of magma ascent through fractures using seismic and geoelectric data

We performed a sequence of synthetic tests simulating magma rising through narrow, vertical fractures. In this first test (Table 1), we simulated a scenario of local anomalies (significant negative variations with respect to a uniform background) of electric resistivity and seismic velocity caused by the magma (or other fluids) rising along vertical conduits (Figure 2, top and bottom left panels show true velocity and resistivity models, respectively). We simulated Earth Resistivity Tomography (ERT) and seismic measurements using a double seismic-geoelectric layout of electric quadrupoles and geophones deployed along the same direction. For geoelectric, we simulated a Wenner-Schlumberger configuration with electrodes fixed every 10 m. Additional electrodes were beyond the left and right borders of the section shown in the figure to expand the maximum available offset with the goal of increasing the sensitivity at greater depth. For seismic simulation, we used geophones equally spaced at 32 m and seismic sources every 160 m (we used a proprietary finite difference forward modeling code for seismic and electric measurements). A horizontal seismic reflector was assumed at a depth of 500 m (not visible in the figure) to have reflected travel times recorded at surface to be used for seismic velocity inversion.

We ran simultaneous self-aware joint inversion of simulated electric potentials and reflection travel times with the scope to detect the changes in resistivity (ρ) and P-velocity (V_p) caused by the rising magma through the fractures. The self-aware joint inversion algorithm identified these changes with good spatial accuracy, as visible in the central panels of the same Figure 2, which represented the inverted velocity (top) and inverted resistivity (bottom) models. We started the inversion using initial velocity-resistivity models derived from the true models perturbed with 100% gaussian noise. The simulated data were contaminated by 10–20% of random noise before the inversion. In Figure 2, the right panels show the percentage difference between true and inverted models. Both inverted velocity and resistivity models reproduce correctly the fracture paths with anomalies reflecting the presence of low velocity/low resistivity values. Errors are very small for the seismic velocity model, focused especially on correspondence of the anomalies of interest; instead, the % error is significantly higher for the retrieved resistivity model (and this is the reason why fractures are more evident in the second case than the first case). This is caused by the fact that we increased the action of the smoothing operator for the geoelectric data inversion, due to the intrinsic lower resolution of this method with respect to the seismic method. However, it is important to note that the most relevant information is contained in the inverted models. In the velocity and resistivity inversions, the reconstructed models reproduce the spatial pattern of the fracture system, demonstrating that the joint inversion framework can recover the major structural and geophysical features of the target despite differences in the accuracy of the recovered physical-property values.

Table 1. Summary of model geometry, layout settings, noise specifications, and parameters for test 1.

Parameter	Value/Description
Model dimensions	1000 m (horizontal) × 500 m (depth)
Background seis. velocity (Vp)	1800 m/s
Background resistivity (ρ)	70 Ω·m
Fracture anomalies	Vp decrease: 10–30%, ρ decrease: 50–70%
Seismic sources spacing	160 m
Seismic geophones spacing	32 m
Geoelectric electrodes	Wenner-Schlumberger, 10 m spacing, extended offsets
Initial model perturbation	Gaussian noise, 100% of true model
Data noise	10–20% random noise
Smoothing factor	Adaptive; higher for resistivity inversion
Cross-gradient weight	0.5 initial, self-adapted during inversion
Maximum iterations	300

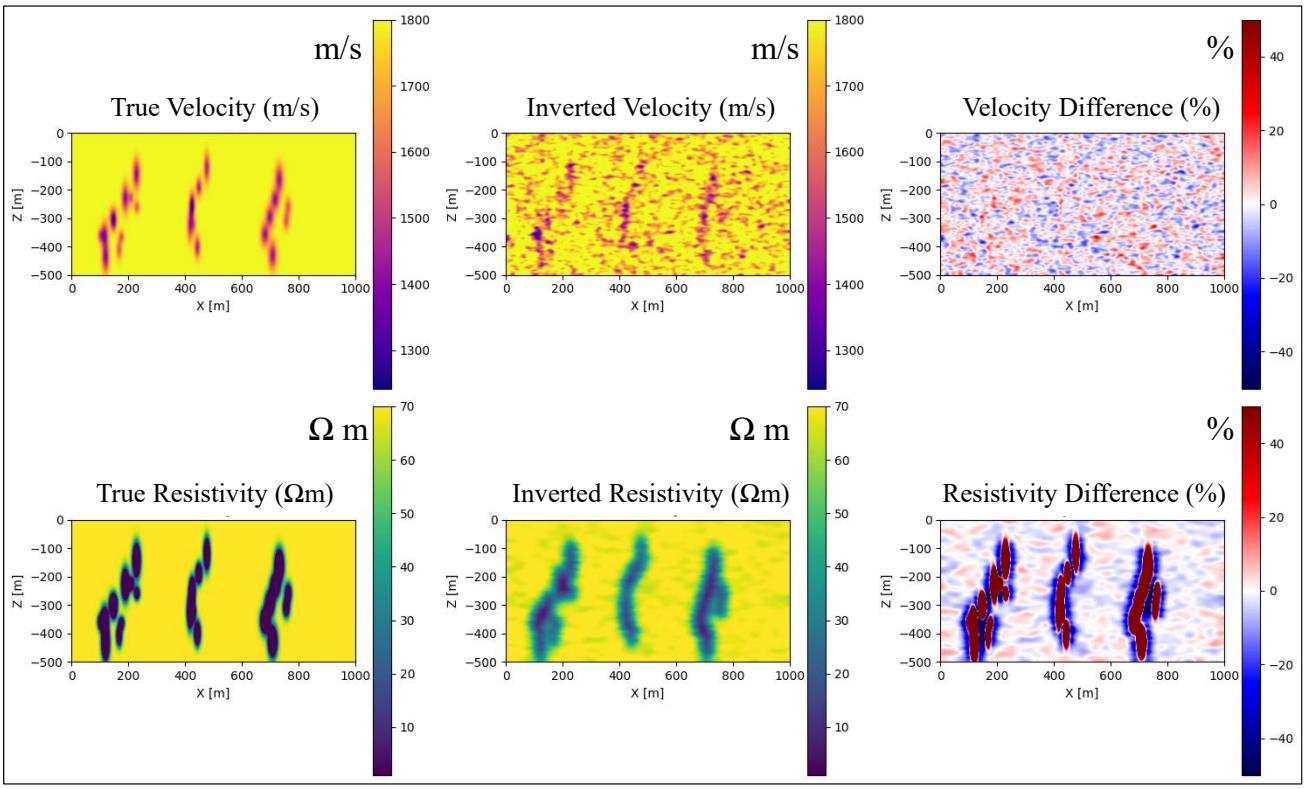

Figure 2. First test. Left panels: true velocity (top) and true resistivity (bottom) models. Central panels: inverted velocity (top) and inverted resistivity (bottom) models. Right panels: differences in % between true and inverted models.

Figure 3 shows the trend of the cost function vs. iteration number for test 1.

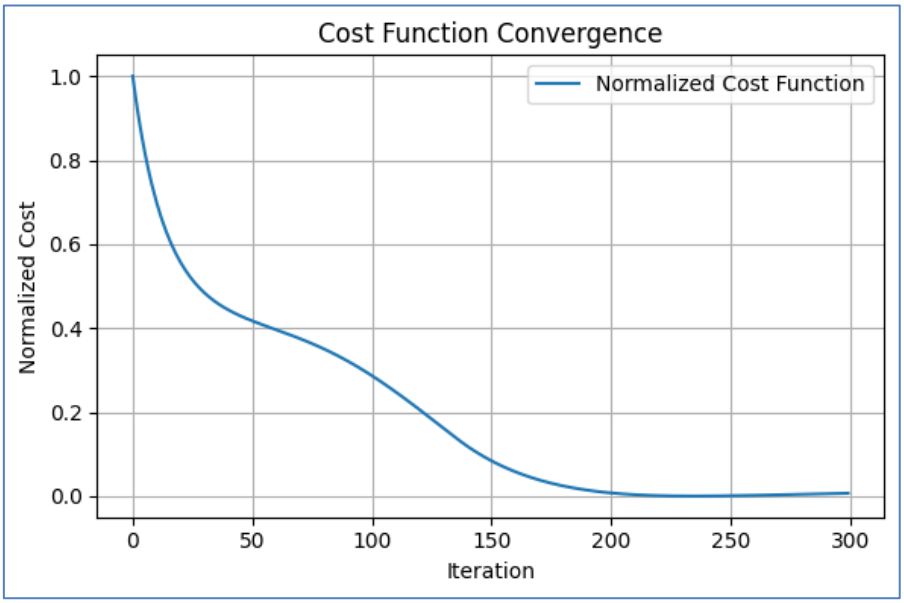

Figure 3. Cost function vs. iteration number for test 1.

3.2. Test 2. Self-aware joint inversion of gravity and electrical data

In the first test, we simulated a joint acquisition of seismic and geoelectric data. This type of dual layout is not always feasible in densely populated areas due to the invasive nature of geophysical surveys using active seismic methods. For that reason, in this second numerical experiment, we tested the self-aware joint inversion approach to simultaneously reconstruct subsurface resistivity and density anomalies from synthetic non-seismic geophysical data. The geophysical responses simulated included apparent resistivities (or electric potentials) typical of geo-electrical or electromagnetic methods (e.g., electrical resistivity tomography, controlled-source electromagnetics, or magnetotellurics), as well as Bouguer gravity anomalies induced by subsurface density contrasts. Our ultimate objective was to evaluate the feasibility and effectiveness of this methodology in time-lapse geophysical monitoring of dynamic volcanic processes, particularly the upward migration of magma through fractures and faults.

3.2.1. Scientific rationale

Resistivity and gravity methods are highly complementary in resolving subsurface structure. In fact, electrical and electric/electromagnetic methods are highly sensitive to fluid content, temperature, and melt fraction, which makes them ideal for detecting magma migration. On the other hand, gravity anomalies provide constraints on subsurface density variations, offering valuable complementary information, especially for relatively low-density magma intrusions. However, these methods traditionally suffer from limited spatial resolution, especially when used independently. This limitation becomes critical in volcanic and geothermal environments, where structural complexity (e.g., faults, fractures, and layered systems) can strongly affect geophysical signatures. To overcome this, we implemented a joint inversion strategy based on the cross-gradient method, where the structural similarity between the resistivity and density models was promoted during the inversion. Additionally,

we assumed that the location and orientation of key fractures and faults had been previously identified via high-resolution seismic imaging or other sources of knowledge (wells, geological surveys, etc.). These geometrical constraints were incorporated into the inversion as structural priors in the starting models, enhancing resolution in the non-seismic domains.

3.2.2. Self-aware inversion framework

In this test, we incorporated, as in the previous test, the self-aware inversion framework, which is capable of automatically adjusting, iteration after iteration, the following hyperparameters: learning rates and smoothing factors, cross-gradient weighting coefficient, balancing structural similarity enforcement, relative weights of the gravity and resistivity misfit terms in the total cost function, inversion mesh resolution, which can be adaptively refined in regions of high sensitivity or uncertainty, and noise adaptation and regularization strength, optimizing the balance between data fidelity and model smoothness. The inversion was governed by a cost function combining misfit terms from both datasets, a cross-gradient structural constraint, and regularization components. Self-awareness was implemented as an adaptive and automatic controller that continuously assessed the inversion quality and updated the hyperparameters accordingly.

3.2.3. Model setup

The true subsurface model consisted of a homogeneous background with density d = 2500 kg/m^3 and resistivity ρ = 200 Ω·m (Table 2). Anomalies representing magma-filled fractures or dykes were included in the model, with decreased density and resistivity with respect to the background. Synthetic data were generated for both datasets by applying simplified forward models using proprietary forward modeling algorithms. To simulate realistic inversion conditions, the initial models used for inversion were built by applying random perturbations up to ±100% to the true models.

3.2.4. Results

After 300 iterations of joint inversion, the resistivity model was recovered in terms of low-resistivity anomalies (Figure 4). Starting from iteration 25, the inversion shows clear and smooth convergence of the cost function (Figure 5). Despite the clear underestimation of the true resistivity values, the low resistivity anomalies caused by the (simulated) ascending magma appear clearly, representing crucial information in the case of a real volcanic risk scenario. The density model also shows useful and interesting information: the major structural features, including the fracture zone containing magma, are delineated in terms of low-density anomalies, even though the geometrical reconstruction is affected by some inaccuracy with respect to the true model. Indeed, the cross-gradient term aligns only partially the structural features in the two models. As such, the cross-gradient term can be balanced for having a better spatial consistency between the resistivity and density models. Moreover, self-aware control mechanism leads to stable convergence and optimal trade-offs between data fitting and model smoothness. These results demonstrate that even with relatively simple acquisition layouts and synthetic data, the self-aware joint inversion successfully enhances resolution and robustness, especially for the electrically conductive and low-density magma-filled zones.

3.2.5. Implications for time-lapse monitoring

This framework is highly suited for time-lapse (4D) geophysical monitoring, especially in volcanic or geothermal systems, where the dynamic movement of magma or fluids needs to be tracked over time. The major advantages include:

- Non-invasive and low-impact acquisition methods: gravity and (electric) electromagnetic methods can be deployed on the surface, with minimal environmental or social disruption.
- Scalability for repeated surveys: the method is ideal for monthly or seasonal campaigns, enabling changes in resistivity and density to be monitored almost continuously.
- Integration with seismic baselines: a single baseline seismic survey (or any other previous information) can provide the geometric constraints needed to anchor the non-seismic inversion, ensuring high spatial resolution without needing repeated seismic acquisitions.

In summary, the self-aware joint inversion approach tested here provides a powerful and flexible tool for integrated subsurface imaging using resistivity and gravity data. When applied in a time-lapse context and constrained by pre-existing (seismic and/or well) data, this method can significantly improve our ability to monitor volcanic systems, detect magma intrusions, and understand fluid dynamics in complex geological environments, as well as in densely populated areas. It opens the door to cost-effective and sustainable geophysical monitoring strategies, with broad implications for hazard assessment and scientific research.

Table 2. Summary of model geometry, layout settings, noise specifications, and parameters for test 2.

Parameter	Value/Description
Model dimensions	1000 m × 500 m
Background density (d)	2500 kg/m³
Background resistivity (ρ)	200 Ω·m
Anomalies (magma-filled fractures)	Density decrease: 5–15%, resistivity decrease: 50–70%
Gravity observation spacing	40 m
Geoelectric acquisition	Simplified ERT/CS-EM, electrode spacing 20 m
Initial model perturbation	±100% random perturbation of true model
Data noise	5–10% random noise
Smoothing factor	Self-adaptive; initially high, reduced iteratively
Cross-gradient weight	0.4 initial, self-adapted
Misfit weights	Balanced automatically by self-aware controller
Maximum iterations	300

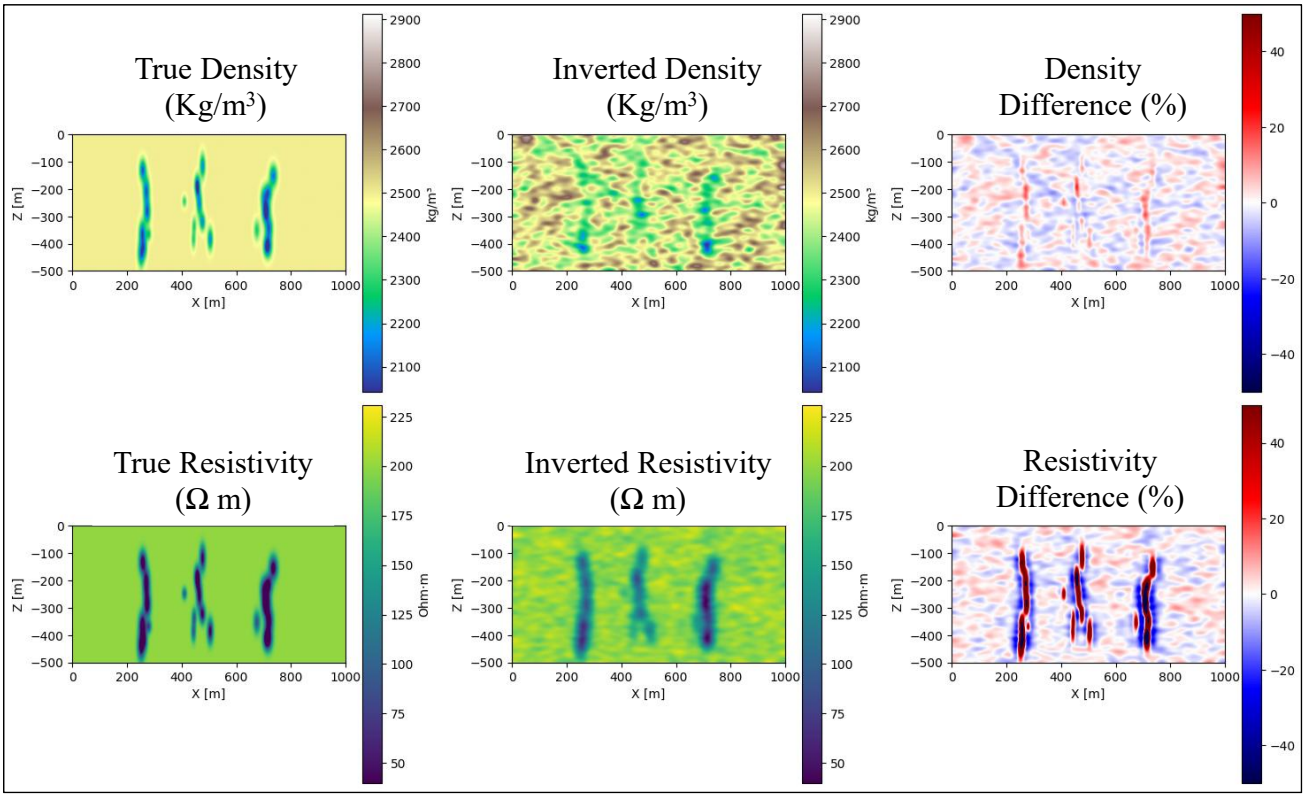

Figure 4. Second test. Left panels: true density (top) and true resistivity (bottom) models. Central panels: inverted density (top) and inverted resistivity (bottom) models. Right panels: differences in % between true and inverted models.

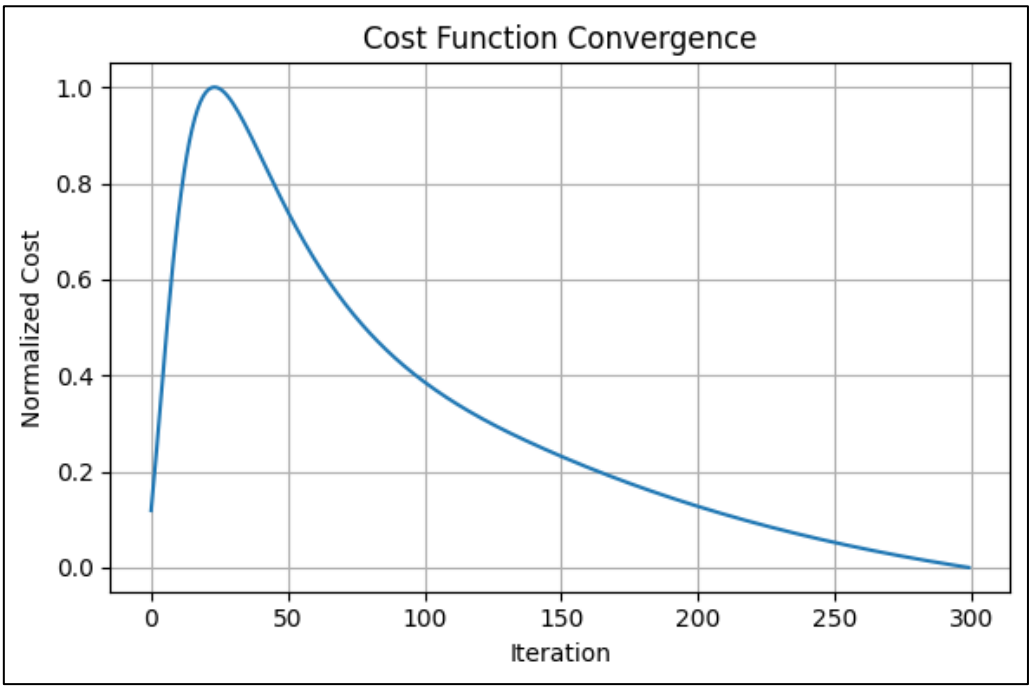

Figure 5. Cost function vs. iteration number for test 2.

3.3. Test 3. Simulation with stratified geological background

In this test, we simulated a more realistic and deeper (down to 1000 m from surface) self-aware joint inversion scenario combining synthetic gravity and electric data. Table 3 includes a schematic summary of model features, layout settings, noise specifications, and key inversion hyper-parameters We began by generating a subsurface model that included a layered geological background and complex, branching anomalies. The background structure mimicked natural layered formations, while the anomalies simulated features such as fractures, dikes, or fluid pathways, branching out in random directions.

From this composite model, synthetic data were generated: the gravity anomaly was simulated from the density distribution, whereas the geoelectric response was simulated using a simplified model that related source-receiver pairs to subsurface resistivity, representing a pseudo-section acquisition like long-offset deep-electrical surveys.

The inversion process then attempted to recover the true subsurface models (density and resistivity) starting from smoothed initial approximations (with 100% random perturbations of the true models). As in the previous tests, the joint inversion used a cross-gradient constraint, which enforced structural similarity between the two models. This constraint ensured that both models evolved to share coherent spatial patterns, promoting geologically plausible results.

A Bayesian-inspired stochastic optimization loop was used to iteratively reduce the data misfit and cross-gradient magnitude. A smoothing operator acted as regularization, and the step sizes (learning rates) adapted dynamically based on whether the model updates improved the misfit.

Throughout the inversion, results were visualized (Figure 6): true models, inverted models, and their percentage differences. A cost function plot tracked the convergence, showing how the inversion learned over time (Figure 7).

Table 3. Summary of model geometry, layout settings, noise specifications, and hyper-parameters for test 3.

Parameter	Value/Description
Model dimensions	1000 m × 1000 m
Background density (d)	Layered: 2500–2700 kg/m³
Background resistivity (ρ)	Layered: 100–300 Ω·m
Anomalies (fractures, dikes, fluid pathways)	Random branching; density decrease: 5–20%, resistivity decrease: 50–80%
Gravity observation spacing	50 m
Geoelectric acquisition	Long-offset pseudo-section, electrodes 20–30 m spacing
Initial model perturbation	100% random perturbation of true model
Data noise	10% random noise
Smoothing factor	Self-adaptive; high at first, reduced during inversion
Cross-gradient weight	0.5 initial, self-adaptive
Misfit weights	Adapted automatically by self-aware inversion
Maximum iterations	200

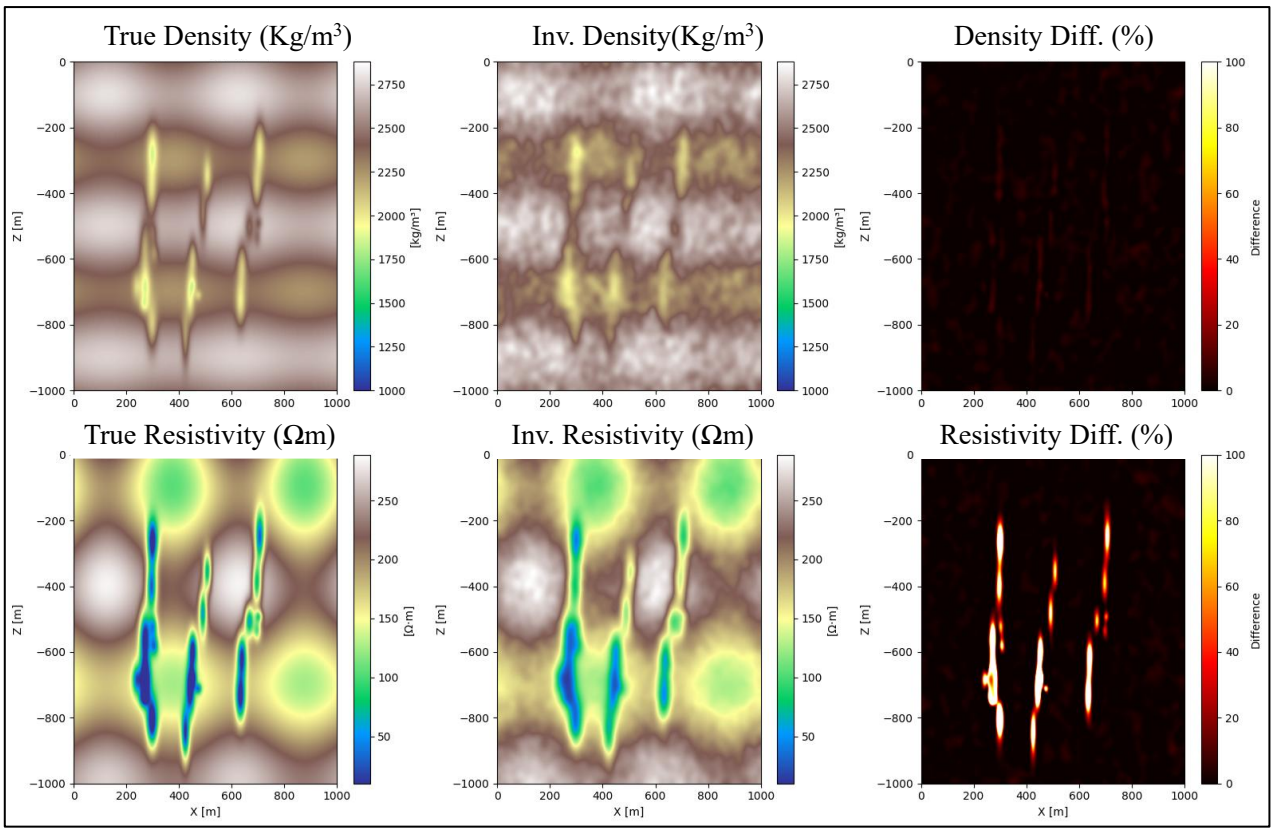

Figure 6. Third test. Left panels: true density (top) and true resistivity (bottom) models. Central panels: inverted density (top) and inverted resistivity (bottom) models. Right panels: differences in % between true and inverted models. Note that the density percentage difference is very small and appears nearly indistinguishable from the background due to the chosen color scale, although it is different from zero.

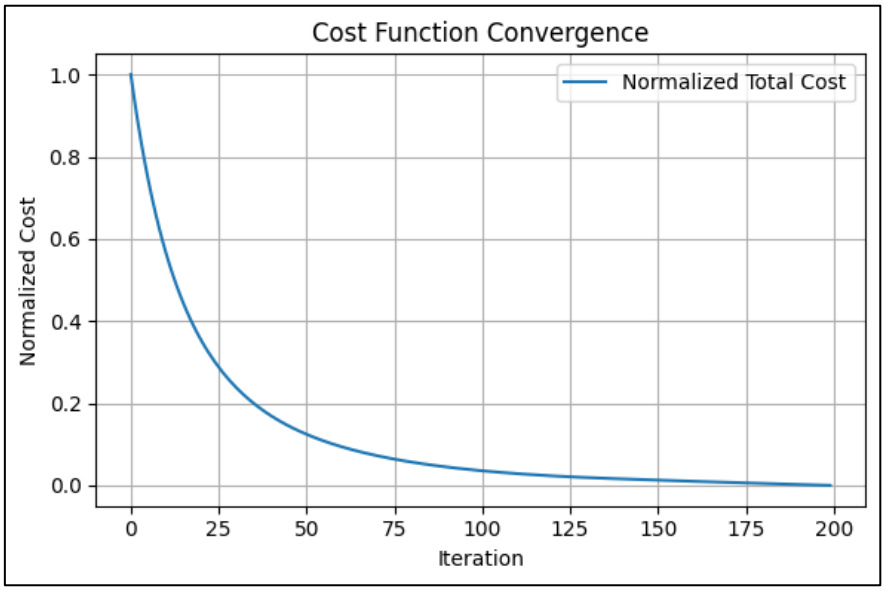

Figure 7. Cost function vs. iteration number for test 3.

4. Discussion and further developments

4.1. Benefits

The simulation tests in the previous section are highly relevant to the field of volcanic hazard assessment and monitoring for several key reasons.

Beyond demonstrating the feasibility of the proposed inversion framework, the results highlight several methodological aspects that are important for the interpretation of multi-physics inversion outputs. The experiments illustrate how the joint inversion process benefits from the complementarity of different geophysical datasets. Seismic, electrical, and gravity measurements respond to different physical properties of the subsurface, and their combined inversion enables structural anomalies to be identified with greater robustness than would be possible using a single method. In particular, the reconstruction of branching anomalies associated with simulated magma pathways demonstrates that even moderate-resolution datasets can provide meaningful structural information when integrated through a consistent inversion framework. Second, the tests emphasize the role of self-regularization and structural constraints in controlling the stability of the inversion. The smoothing operators help suppress unrealistic oscillations in the recovered models, especially in the early stages of the optimization process, while the cross-gradient constraint promotes structural coherence between the physical property models. The balance between these components is essential for obtaining geologically plausible solutions. Finally, the results show that the adaptive hyperparameter self-adjustment mechanism plays an important role in maintaining stable convergence. By automatically adapting learning rates, smoothing factors, and relative weights between the misfit terms, the algorithm can respond to the evolving behavior of the cost function and progressively refine the model updates. This self-adaptive strategy reduces the need for manual tuning and improves the robustness of the inversion when dealing with complex multi-physics datasets.

In a more general sense, our tests indicate the potential for joint acquisition and joint inversion of multi-physics geodata to reconstruct branched anomalies that can be crucial for detecting and monitoring magma ascent through deep, fractured rock. These patterns are typical of dyke swarms, sill complexes, or magma fingers that may precede eruptive phases. Our approach has clear “early warning” capabilities. In fact, by identifying magma movement before it reaches the surface, this method can contribute to early warning systems. It can enhance our capacity to predict eruptive activity by detecting subsurface changes in density, resistivity, or seismic velocity associated with fluid migration or thermal anomalies.

However, we must remark that, while seismic acquisition is highly informative, it can be too intrusive, especially in densely populated volcanic regions. In fact, seismic acquisition has generally significant environmental impact, produces strong ground vibrations, has generally high logistical cost, and so forth. For that reason, we have proposed complementing seismic acquisition with gravity and geoelectrical data, which offer high acquisition frequency (weekly or monthly), minimal environmental impact, relatively low operational cost, and safe deployment in populated areas. Moreover, the same self-aware joint inversion framework can be extended to joint inversion of other types of measurements, such as gravity gradiometer and magnetotelluric data, which are sensitive to density-resistivity contrasts, such as those caused by magma, fluids, or hydrothermal systems. To limit the impact of seismic data campaigns, these can be acquired through a unique baseline survey, at

specific locations, to provide all the necessary geometrical constraints (high resolution spatial model of the subsurface) to support constrained joint inversion of non-seismic data. This combined approach enhances spatial resolution and model reliability, exploits the complementary sensitivity of each data type, and enables continuous monitoring using portable, non-invasive sensors.

Future developments and extensions of this approach can be envisioned in multiple directions. First, the joint inversion methodology can be further enhanced by integrating additional geoscientific data sources, such as geological constraints (e.g., structural maps and stratigraphic logs), borehole measurements, and hydrogeological information. These datasets can serve as priors or constraints during the inversion process, reducing non-uniqueness and improving the geological plausibility of the results.

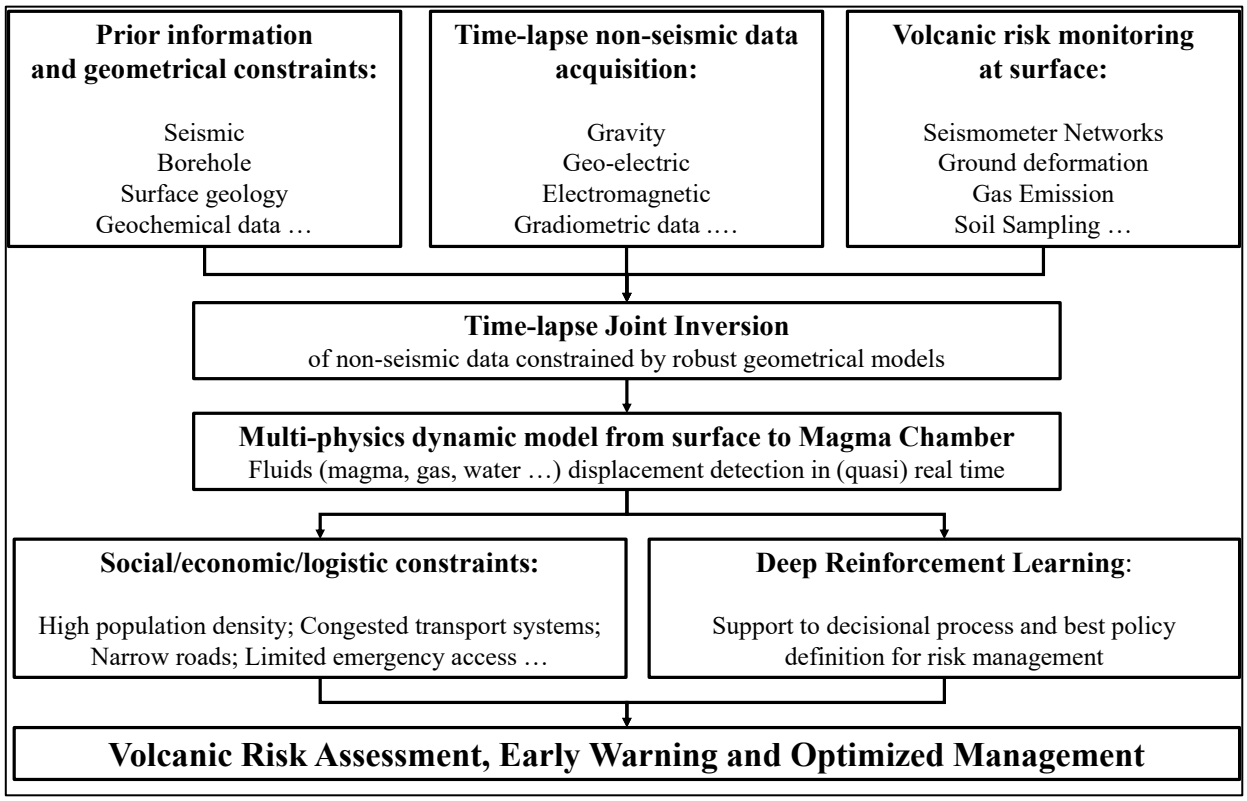

Figure 8. General scheme of the holistic approach for dynamic definitions of volcanic risk, early warning, and optimal decisional policy in densely populated areas.

Moreover, the integration of advanced artificial intelligence techniques, including deep learning and reinforcement learning, opens new opportunities for combining the results of integrated geophysical models with a wide range of ancillary data. The proposed approach could be significantly improved by integrating additional types of observations, such as geochemical measurements and other independent datasets, which may provide complementary constraints on subsurface processes. In that multidisciplinary frame, deep learning algorithms can play a key role. By training AI models to recognize patterns across such multi-modal datasets, it becomes possible to extract higher-level insights about the state of the subsurface and the dynamic processes occurring in volcanic, geothermal, or tectonically active areas.

Furthermore, reinforcement learning can be used to develop intelligent agents capable of defining optimal risk management strategies. These agents could simulate and evaluate intervention policies under varying scenarios, considering all available variables, including physical, geochemical, and geophysical indicators, as well as socio-economic constraints and territorial characteristics specific to the region under investigation. This holistic and adaptive approach is summarized in Figure 8. This can significantly enhance the ability of decision-makers to anticipate and mitigate geohazards and to define evidence-based policies for sustainable territorial management.

4.2. Limitations

While the approach presented in this study offers several advantages and potential benefits, it is also important to recognize that it presents several limitations and methodological constraints that should be considered. First, the performance of the inversion remains strongly dependent on the quality, coverage, and noise level of the input datasets. As in any geophysical inversion problem, incomplete acquisition geometry or poor signal-to-noise ratio may reduce the resolution of the reconstructed models and potentially introduce ambiguities in the recovered physical-property distributions.

A second limitation concerns the balance between data fitting and structural coupling. The use of cross-gradient constraints and smoothing operators improves the structural consistency between the different physical-property models, but it may also introduce a degree of bias toward common structural patterns. In situations where the physical properties are only partially correlated, an excessively strong coupling term could potentially suppress genuine differences between the models. Careful tuning of the regularization parameters therefore remains a critical aspect of the inversion strategy.

Finally, the results shown in Figure 5 provide useful insight into the convergence behavior of the algorithm through the evolution of the corresponding cost functions. The decrease of the cost function becomes evident only after approximately iteration 25. This behavior can be explained by the presence of an initial exploratory phase of the optimization process. During the first iterations, the algorithm explores the model space and tests different parameter configurations, which can temporarily lead to an increase in the misfit and therefore to a peak in the cost function. Around iteration 25, the algorithm identifies a region of the model space that is closer to the optimal solution. The peak observed at this iteration corresponds to a transition point between the exploratory phase and the convergence phase. After this point, the update mechanism becomes more effective in reducing the discrepancy between observed and predicted data, leading to a systematic decrease in the cost function and a progressive convergence of the inversion process toward a better solution.

4.3. Structural recovery versus absolute property estimation

It is also worth noting that the cost-function evolution reflects the inherent trade-off between accurate recovery of absolute physical-property values and reconstruction of the major structural features of the subsurface. In the synthetic tests presented here, the inversion successfully reproduces the spatial distribution and geometry of the fracture system, even when the absolute values of some physical parameters are not perfectly recovered. From a monitoring perspective, the reliable reconstruction of structural patterns and anomaly distributions is often more relevant than the exact recovery of the physical-property amplitudes.

These results therefore suggest that the proposed framework can effectively identify structurally consistent anomalies across datasets, although its performance in real monitoring scenarios will inevitably depend on data availability, constraints from prior information, survey design, and the appropriate selection of inversion parameters.

5. Conclusions

The methodology introduced in this paper presents an adaptive framework for the joint inversion of multi-physics geophysical datasets, with potential applications in monitoring complex volcanic systems. The main contribution of this work lies in the development of a self-aware joint inversion strategy capable of dynamically adjusting key hyperparameters during the optimization process to improve convergence stability and model consistency.

By integrating multi-domain, non-invasive geophysical data through the Self-Aware Joint Inversion technique, our method enables continuous, high-resolution imaging of subsurface processes in inhabited areas where traditional monitoring strategies often fall short, especially in densely populated or socio-economically fragile settings. This paradigm shift not only enhances early warning systems and supports proactive risk mitigation but also provides decision-makers with actionable insights that are sensitive to the complexity of social vulnerability, spatial inequalities, and governance challenges.

In the general context of increasing exposure to natural hazards due to climate change, urbanization, and global socio-economic transformations, the proposed methodology addresses the urgent need for adaptive, inclusive, and high-resolution tools capable of anticipating subsurface processes before they manifest at the surface. Importantly, it contributes to rethinking volcanic risk assessment not merely as a technical exercise, but as a socially embedded practice that must account for the capacities of communities to cope with, respond to, and recover from disasters.

At this stage, the methodology has been evaluated exclusively using synthetic data generated from realistic volcanic scenarios. We acknowledge that the main limitation of this study is the lack of validation on real data. However, our controlled experiments have provided a rigorous assessment of the system's performance, adaptability, and resolution under complex, multi-parameter conditions. While the results are encouraging, validation on real-world datasets remains a crucial next step to fully establish the operational potential of the approach, especially in socially diverse and infrastructurally constrained volcanic areas. In future work, we will focus on applying the method to field measurements as soon as they become available, ideally in collaboration with suitably equipped university research centers or specialized institutions, to ensure a scientifically robust demonstration of its applicability in real volcanic risk monitoring and management.

Nonetheless, even in this initial phase, our findings point to the high potential for quantitative integration of diverse geophysical datasets, including seismic, electrical, electromagnetic, and gravity measurements, into a unified inversion framework. This capability enables the construction of detailed, multiparametric models of the subsurface that not only improve forecasting accuracy but also support the visualization of territorial vulnerabilities and the co-design of inclusive mitigation strategies.

In doing so, the proposed methodology advances the scientific understanding of volcanic systems and the broader agenda of disaster risk reduction. Additionally, it promotes a more informed response to geohazards by combining high-resolution geophysical imaging and machine learning with an

awareness of the intersecting social, economic, and environmental factors that define vulnerability across scales.

Use of AI tools declaration

The authors declare they have not used Artificial Intelligence tools in the creation of this article.

Acknowledgments

This research and this paper were conducted without any funding, solely during the author's private time and using the author's personal resources.

Conflict of interest

The Author declares that this research was conducted entirely in his private time, using exclusively personal methodologies, software, and other proprietary tools, and relying solely on synthetic data that is his own property.

Appendix. Theoretical formulation of Self-Aware Joint Inversion (SAJI)

In this Appendix, we provide a formal description of the Self-Aware Joint Inversion (SAJI) framework adopted in this study. The method extends multi-physics joint inversion by introducing a self-adaptive control of hyperparameters based on the evolution of the global objective function. More detailed discussions of the general self-aware methodology are reported in other studies [43,44].

The aim of SAJI is to simultaneously invert multiple geophysical datasets to retrieve a physically consistent multi-parameter model while dynamically adjusting the inversion strategy to improve convergence, robustness, and stability.

A.1. Model parameterization and forward problem

Let

$$\boldsymbol{\Omega} \subset \mathbb{R}^{\mathbf{3}}$$

denote the spatial domain of the inversion.
The joint model vector is defined as

$$\boldsymbol{m} = \begin{bmatrix} \boldsymbol{m}_{\mathbf{velocity}} \\ \boldsymbol{m}_{\mathbf{resistivity}} \\ \boldsymbol{m}_{\mathbf{density}} \end{bmatrix}$$

where

- $\boldsymbol{m}_{\mathbf{velocity}}(\mathbf{x})$ is the seismic velocity model.
- $\boldsymbol{m}_{\mathbf{resistivity}}(\mathbf{x})$ is the electrical resistivity model.
- $\boldsymbol{m}_{\mathbf{density}}(\mathbf{x})$ is the bulk density model.

with $\mathbf{x} \in \boldsymbol{\Omega}$.
At iteration n of the inversion, the model estimate is denoted by

$$\boldsymbol{m}^{(n)}.$$

For each geophysical domain *i*, the predicted data is obtained through the forward operator

$$\boldsymbol{d}_{\boldsymbol{i}}^{(n)} = \boldsymbol{g}_{\boldsymbol{i}}(\boldsymbol{m}_{\boldsymbol{i}}{}^{(n)})$$

where

- $\boldsymbol{g}_{\boldsymbol{i}}(\cdot)$ is the forward modeling operator.
- $i \in$ {seismic, electric/electromagnetic, gravity domains

Examples include:

- Seismic travel-time or reflection modeling.
- Electrical potential modeling for geoelectrical data.
- Gravity response modeling for density.

The complete predicted data vector is therefore

$$\boldsymbol{d}^{(n)} = \boldsymbol{g}(\boldsymbol{m}^{(n)}).$$

A.2. Joint objective function

The inversion seeks the model minimizing the joint cost functional

$$\Phi_{\text{joint}}(\boldsymbol{m}) = \lambda_1\Phi_{\text{mis}} + \lambda_2\Phi_{\text{reg}} + \lambda_3\Phi_{\text{X}} + \lambda_4\Phi_{\text{analytic}}$$

where

Φ_{mis} is the total data misfit term.

Φ_{reg} is the regularization term.

Φ_{X} is the structural coupling (cross-gradient).

Φ_{analytic} enforces analytical or petrophysical relations.

λ_{i} are weighting coefficients (see Section 2.2).

A.2.1. Data misfit term

The misfit term measures the discrepancy between observed and predicted data:

$$\Phi_{\text{mis}} = \sum_{\boldsymbol{i}} \| \mathbf{W}_{\boldsymbol{i}}\left(\boldsymbol{d}_{\boldsymbol{i}}^{\text{obs}} - \boldsymbol{g}_{\boldsymbol{i}}(\boldsymbol{m})\right) \|^{\mathbf{2}}$$

where

- $\boldsymbol{d}_{\boldsymbol{i}}^{\text{obs}}$ are observed data.
- $\mathbf{W}_{\boldsymbol{i}}$ is the data weighting matrix.

A.2.2. Regularization term

To stabilize the inversion, spatial regularization is applied. In this implementation, this corresponds to adaptive Gaussian smoothing, expressed as

$$\Phi_{\text{reg}} = \sum_{\boldsymbol{i}} \| \boldsymbol{\nabla m}_{\boldsymbol{i}} \|^{\mathbf{2}}$$

with

$$i \in \{\text{velocity, resistivity, density}\}.$$

Operationally, smoothing is applied through a Gaussian filtering operator

$$\tilde{\boldsymbol{m}}_{\boldsymbol{i}}^{(\boldsymbol{n})} = \boldsymbol{G}(\boldsymbol{m}_{\boldsymbol{i}}^{(\boldsymbol{n})}, s_{\boldsymbol{n}})$$

where

- $\boldsymbol{G}(\cdot)$ is a Gaussian smoothing operator.
- s_n is the smoothing factor at iteration n.

A.3. Structural coupling: cross-gradient constraint

To enforce structural consistency between models derived from different physical parameters, a cross-gradient constraint is introduced. For two model parameters, $\boldsymbol{m_i}$ and $\boldsymbol{m_j}$, the cross-gradient functional is defined as

$$\Phi_{\mathrm{X}} = \int_{\boldsymbol{\Omega}} \| \boldsymbol{\nabla m_i} \times \boldsymbol{\nabla m_j} \|^2 \ \boldsymbol{d\Omega}.$$

For instance, the coupling applied between seismic velocity and electrical resistivity is:

$$\Phi_{\mathrm{X}} = \int_{\boldsymbol{\Omega}} \| \boldsymbol{\nabla m}_{\mathbf{velocity}} \times \boldsymbol{\nabla m}_{\mathbf{resistivity}} \|^2 \ \boldsymbol{d\Omega}.$$

The cross-gradient tends toward zero when the spatial gradients of the models are parallel, meaning that structural interfaces coincide across physical domains.

A.4. Analytical (petrophysical) constraint

An additional constraint can be introduced through analytical rock-physics relationships linking physical parameters, such as

$$\boldsymbol{m}_{\mathbf{density}} = \boldsymbol{f}(\boldsymbol{m}_{\mathbf{velocity}}, \boldsymbol{m}_{\mathbf{resistivity}})$$

where $\boldsymbol{f}(\cdot)$ represents a petrophysical model derived from laboratory or other empirical relationships. The associated penalty term is

$$\Phi_{\text{analytic}} = \int_{\boldsymbol{\Omega}} \left(\boldsymbol{m}_{\mathbf{density}} - \boldsymbol{f}(\boldsymbol{m}_{\mathbf{velocity}}, \boldsymbol{m}_{\mathbf{resistivity}})\right)^2 \ \boldsymbol{d\Omega}.$$

This term ensures physical consistency between the inverted parameters.

A.5. Model update

The model parameters are iteratively updated by minimizing the joint objective function.
In a gradient-based formulation:

$$\boldsymbol{m}^{(\boldsymbol{n+1})} = \boldsymbol{m}^{(\boldsymbol{n})} - \boldsymbol{\eta}^{(\boldsymbol{n})} \odot \boldsymbol{\nabla}_{\boldsymbol{m}} \Phi_{\text{joint}}(\boldsymbol{m}^{(\boldsymbol{n})})$$

where

- $\odot$ denotes element-wise multiplication.
- $\boldsymbol{\eta}^{(\boldsymbol{n})}$ is the vector of learning rates.

$$\boldsymbol{\eta}^{(n)} = \begin{bmatrix} \boldsymbol{\eta}_{\text{seis}}^{(n)} \\ \boldsymbol{\eta}_{\text{res}}^{(n)} \\ \boldsymbol{\eta}_{\text{dens}}^{(n)} \end{bmatrix}.$$

Alternatively, the update step can be formulated within a Bayesian framework by maximizing the posterior probability distribution

$$\mathrm{p}(\boldsymbol{m} \mid \boldsymbol{d}) \propto \mathrm{p}(\boldsymbol{d} \mid \boldsymbol{m})\, \mathrm{p}(\boldsymbol{m})$$

A.6. Self-aware hyperparameter adaptation

The key innovation of SAJI is the dynamic self-adjustment of hyperparameters according to the evolution of the global cost function.

A generic adaptive rule for a learning rate $\boldsymbol{\eta}$ can be expressed as

$$\boldsymbol{\eta}^{(n+1)} = \begin{cases} \alpha \boldsymbol{\eta}^{(n)} & \text{if } \Phi_{joint}^{(n)} < \Phi_{joint}^{(n-1)} - \varepsilon \\ \beta \boldsymbol{\eta}^{(n)} & \text{otherwise} \end{cases}$$

where

- $\alpha > 1$ increases the learning rate when convergence improves.
- $0 < \beta < 1$ reduces the learning rate otherwise.
- ε is a tolerance threshold.

For example

$$\alpha = 1.05; \quad \beta = 0.7.$$

Similar adaptive rules are applied to other hyperparameters, including

- smoothing factor $s_{\boldsymbol{n}}$.
- Cross-gradient weight λ_3.
- Regularization weights.

This feedback mechanism enables the inversion process to self-regulate its optimization dynamics.

A.7. Iterative inversion scheme

The complete SAJI workflow consists of the following steps:

1. Initialize model $\boldsymbol{m}^{(0)}$ and the hyperparameters.
2. Compute predicted data $\boldsymbol{g}(\boldsymbol{m}^{(n)})$.
3. Evaluate the joint cost function $\Phi_{joint}^{(n)}$.
4. Update hyperparameters according to the self-aware rules.
5. Compute gradients of the objective function.
6. Update model parameters.
7. Apply adaptive smoothing.
8. Repeat until convergence.

Convergence may be defined as

$$| \Phi_{joint}^{(n)} - \Phi_{joint}^{(n-1)} | < \varepsilon$$

or by stabilization of the posterior probability in a Bayesian formulation.

A.8. Conceptual interpretation

The SAJI framework can be interpreted as a self-regulated optimization system in which the inversion dynamically adjusts its own hyperparameters to improve stability and convergence.
This approach offers several advantages:

- Improved convergence speed.
- Adaptive regularization.
- Robustness to noisy data.
- Enhanced structural consistency across geophysical domains.

As a result, the retrieved multi-parameter models are physically plausible, structurally coherent, and computationally efficient to obtain.

A.9. Simplified pseudocode

To better clarify the internal logic of the self-aware joint inversion strategy, we present below a simplified Python-style pseudocode. The key idea is to adaptively adjust (without any direct human action) the most critical hyperparameters, such as learning rates, smoothing factors, and constraint-misfit weights, based on the global behavior of the cost function during the joint inversion process. For completeness, Table A.1 shows the Self-Aware JI key hyperparameters.

Pseudocode

```
# Initialize inversion parameters and hyperparameters (like earlier, values here are just examples)
learning_rate_seismic = 0.01
learning_rate_resistivity = 0.01
smoothing_factor = 1.0
cross_gradient_weight = 0.5
previous_cost = float('inf')
patience = 5
tolerance = 1e-4

for iteration in range(max_iterations):

    # Step 1: Forward modeling for both domains
    predicted_seismic = forward_model_seismic(model_velocity)
    predicted_resistivity = forward_model_resistivity(model_resistivity)

    # Step 2: Compute cost terms
    cost_seismic = compute_misfit(predicted_seismic, observed_seismic)
    cost_resistivity = compute_misfit(predicted_resistivity, observed_resistivity)
```

```
cross_gradient_term = compute_cross_gradient(model_velocity, model_resistivity)

total_cost = cost_seismic + cost_resistivity + cross_gradient_weight * cross_gradient_term

# Step 3: Adjust learning rate based on cost evolution
 # This is just an example of self-adjustment as a function of the cost function
if total_cost < previous_cost - tolerance:
    learning_rate_seismic *= 1.05
    learning_rate_resistivity *= 1.05
    smoothing_factor *= 0.95
    cross_gradient_weight *= 1.02
else:
    learning_rate_seismic *= 0.7
    learning_rate_resistivity *= 0.7
    smoothing_factor *= 1.05
    cross_gradient_weight *= 0.98

# Step 4: Compute gradients and update models
grad_velocity = compute_gradient(cost_seismic, model_velocity)
grad_resistivity = compute_gradient(cost_resistivity, model_resistivity)

model_velocity -= learning_rate_seismic * grad_velocity
model_resistivity -= learning_rate_resistivity * grad_resistivity

# Step 5: Apply smoothing
model_velocity = gaussian_smoothing(model_velocity, smoothing_factor)
model_resistivity = gaussian_smoothing(model_resistivity, smoothing_factor)

# Step 6: Update cost history
previous_cost = total_cost

# Diagnostics
if iteration % 50 == 0:
    print(f'Iteration {iteration} | Cost: {total_cost:.4f}")
```

Table A.1. Self-Aware JI key hyperparameters' adjustment.

Hyperparameter	Symbol	Function	Adjustment Logic
Learning rate (Seis)	learning_rate_seismic	Controls update step size for seismic model	Increases if cost decreases; decreases if cost worsens
Learning rate (Res)	learning_rate_resistivity	Controls update step size for resistivity model	Same as above
Smoothing factor	smoothing_factor	Regulates spatial smoothing of model parameters	Decreased when cost improves to allow sharper features
Cross-gradient weight	cross_gradient_weight	Enforces structural similarity between velocity and resistivity models	Increased when models align; decreased if structural misfit grows
Cost function	total_cost	Aggregate cost including misfit terms, their relative weights and cross-gradient	Used to trigger dynamic changes in other hyperparameters
Patience/Tolerance	tolerance	Threshold for determining if cost improvement is significant	Prevents hyperparameter changes on small fluctuations

References

1. Barberi F, Bertagnini A, Landi P, et al. (1992) A review on phreatic eruptions and their precursors. *J Volcanol Geotherm Res* 52: 231–246. https://doi.org/10.1016/0377-0273(92)90046-G
2. Saccorotti G, Lokmer I (2021) A review of seismic methods for monitoring and understanding active volcanoes. In: Papale P, Ed., *Forecasting and Planning for Volcanic Hazards, Risks, and Disasters*, Elsevier, 25–73. https://doi.org/10.1016/B978-0-12-818082-2.00002-0
3. Di Bella GS (2025) AI-based multi-sensor data fusion for near real-time monitoring of effusive volcanic activity: A case study of Mount Etna (November 2022–February 2023). *Ann Geophys* 68: V221. https://doi.org/10.4401/ag-9185
4. Del Negro C, Cappello A, Bilotta G, et al. (2020) Living at the edge of an active volcano: Risk from lava flows on Mt Etna. *Geol Soc Am Bull* 132: 1615–1625. https://doi.org/10.1130/B35290.1
5. Piochi M, Cantucci B, Montegrossi G, et al. (2021) Hydrothermal alteration at the San Vito area of the Campi Flegrei geothermal system in Italy: Mineral review and geochemical modeling. *Minerals* 11: 810. https://doi.org/10.3390/min11080810
6. Piochi M, Mastrolorenzo G, Pappalardo L (2005) Magma ascent and eruptive processes from textural and compositional features of Monte Nuovo pyroclastic products, Campi Flegrei, Italy. *Bull Volcanol* 67: 663–678. https://doi.org/10.1007/s00445-005-0410-1
7. Rouwet D, Sandri L, Marzocchi W, et al. (2014) Recognizing and tracking volcanic hazards related to non-magmatic unrest: A review. *J Appl Volcanol* 3: 17. https://doi.org/10.1186/s13617-014-0017-3
8. Cigna F, Tapete D, Lu Z (2020) Remote sensing of volcanic processes and risk. *Remote Sens* 12: 2567. https://doi.org/10.3390/rs12162567

9. Loughlin SC, Sparks S, Brown SK, et al. (2015) *Global Volcanic Hazards and Risk*. Cambridge University Press. https://doi.org/10.1017/CBO9781316276273
10. Ebmeier SK, Andrews BJ, Araya MC, et al. (2018) Synthesis of global satellite observations of magmatic and volcanic deformation: Implications for volcano monitoring and the lateral extent of magmatic domains. *J Appl Volcanol* 7: 1–26. https://doi.org/10.1186/s13617-018-0071-3
11. Pyle DM, Mather TA, Biggs J (2013) Remote sensing of volcanoes and volcanic processes: Integrating observation and modelling—Introduction. *Geol Soc Spec Publ* 380: 1–13. https://doi.org/10.1144/SP380.1
12. Francis PW (1989) Remote sensing of volcanoes. *Adv Space Res* 9: 89–92. https://doi.org/10.1016/0273-1177(89)90471-7
13. Sansivero F, Vilardo G (2019) Processing thermal infrared imagery time-series from volcano permanent ground-based monitoring network. *Remote Sens* 11: 553. https://doi.org/10.3390/rs11050553
14. Laiolo M, Ripepe M, Cigolini C, et al. (2019) Space- and ground-based geophysical data tracking of magma migration in the shallow feeding system of Mount Etna volcano. *Remote Sens* 11: 1182. https://doi.org/10.3390/rs11101182
15. Alperovich L, Eppelbaum L, Zheludev V, et al. (2013) A new combined wavelet methodology applied to GPR and ERT data in the Montagnole experiment. *J Geophys Eng* 10: 025017. https://doi.org/10.1088/1742-2132/10/2/025017
16. Mallat S (1999) *A Wavelet Tour of Signal Processing*, Academic Press.
17. Daubechies I (1992) *Ten Lectures on Wavelets*, Society for industrial and applied mathematics.
18. Tarantola A (2005) *Inverse Problem Theory and Methods for Model Parameter Estimation*, Society for industrial and applied mathematics.
19. Mosegaard K, Tarantola A (1995) Monte Carlo sampling of solutions to inverse problems. *J Geophys Res* 100: 12431–12447. https://doi.org/10.1029/94JB03097
20. Sambridge M, Mosegaard K (2002) Monte Carlo methods in geophysical inverse problems. *Rev Geophys* 40: 3-1–3-29. https://doi.org/10.1029/2000RG000089
21. Gallardo LA, Meju MA (2003) Characterization of heterogeneous near-surface materials by joint 2D inversion of DC resistivity and seismic data. *Geophys Res Lett* 30. https://doi.org/10.1029/2003GL017370
22. Gallardo LA, Meju MA (2004) Joint two-dimensional DC resistivity and seismic travel time inversion with cross-gradients constraints. *J Geophys Res* 109: B03311. https://doi.org/10.1029/2003JB002716
23. Haber E, Oldenburg DW (1997) Joint inversion: A structural approach. *Inverse Probl* 13: 63–77. https://doi.org/10.1088/0266-5611/13/1/006
24. Linde N, Tryggvason A, Peterson JE, et al. (2008) Joint inversion of crosshole radar and seismic traveltimes acquired at the South Oyster bacterial transport site. *Geophysics* 73: G29–G37. https://doi.org/10.1190/1.2937467
25. Bergen KJ, Johnson PA, de Hoop MV, et al. (2019) Machine learning for data-driven discovery in solid Earth geoscience. *Science* 363: eaau0323. https://doi.org/10.1126/science.aau0323
26. Yu S, Ma J (2021) Deep learning for geophysics: Current and future trends. *Rev Geophys* 59: e2021RG000742. https://doi.org/10.1029/2021RG000742

27. Araya, M. (2021) Deep Learning for Seismic Inverse Problems: Toward the Acceleration of Geophysical Analysis Workflows. *IEEE Signal Process Mag*. https://doi.org/10.1109/MSP.2020.3037429
28. Dell'Aversana P (2025) Self-aware joint inversion of multidisciplinary geophysical data in mineral exploration using hyperparameter self-adjustment: A preliminary study. *Minerals* 15: 623. https://doi.org/10.3390/min15060623
29. Vozoff K, Jupp DLB (1975) Joint inversion of geophysical data. *Geophys J Int* 42: 977–991. https://doi.org/10.1111/j.1365-246X.1975.tb06462.x
30. Colombo D, McNeice G, Raterman N, et al. (2014) Massive integration of 3D EM, gravity and seismic data for deepwater subsalt imaging in the Red Sea. *SEG International Exposition and Annual Meeting*.
31. Dell'Aversana P (2014) *Integrated Geophysical Models: Combining Rock Physics with Seismic, Electromagnetic and Gravity Data*, EAGE Publications.
32. Doetsch J, Linde N, Binley A (2010) Structural joint inversion of time-lapse crosshole ERT and GPR traveltime data. *Geophys Res Lett* 37: L24404. https://doi.org/10.1029/2010GL045482
33. Doetsch J, Linde N, Coscia I, et al. (2010) Zonation for 3D aquifer characterization based on joint inversions of multimethod crosshole geophysical data. *Geophysics* 75: G53–G64. https://doi.org/10.1190/1.3496476
34. Hamdan HA, Vafidis A (2013) Joint inversion of 2D resistivity and seismic travel time data to image saltwater intrusion over karstic areas. *Environ Earth Sci* 68: 1877–1885. https://doi.org/10.1007/s12665-012-1875-9
35. Hellman K, Ronczka M, Günther T, et al. (2017) Structurally coupled inversion of ERT and refraction seismic data combined with cluster-based model integration. *J Appl Geophys* 143: 169–181. https://doi.org/10.1016/j.jappgeo.2017.06.008
36. Infante V, Gallardo LA, Montalvo-Arrieta JC, et al. (2010) Lithological classification assisted by the joint inversion of electrical and seismic data. *J Appl Geophys* 70: 93–102. https://doi.org/10.1016/j.jappgeo.2009.11.003
37. Moorkamp M, Jones AG, Eaton DW (2007) Joint inversion of teleseismic receiver functions and magnetotelluric data using a genetic algorithm. *Geophys Res Lett* 34: L16311. https://doi.org/10.1029/2007GL030519
38. Shi Z, Hobbs RW, Moorkamp M, et al. (2017) 3-D cross-gradient joint inversion of seismic refraction and DC resistivity data. *J Appl Geophys* 141: 54–67. https://doi.org/10.1016/j.jappgeo.2017.04.008
39. Miotti F, Zerilli A, Menezes PTL, et al. (2018) A new petrophysical joint inversion workflow: Advancing reservoir characterization challenges. *Interpretation* 6: SG33–SG39. https://doi.org/10.1190/INT-2017-0225.1
40. Miotti F, Rovetta D, Bernasconi G (2009) Joint inversion of well-log data. *SEG Tech Program Expand Abstr*, 2218–2222. https://doi.org/10.1190/1.3255301
41. De Stefano M, Golfré Andreasi F, Re S, et al. (2011) Multiple-domain simultaneous joint inversion of geophysical data with application to subsalt imaging. *Geophysics* 76: R69–R80. https://doi.org/10.1190/1.3554652

42. Dell'Aversana P, Bernasconi G, Miotti F, et al. (2011) Joint inversion of rock properties from sonic, resistivity and density well-log measurements. *Geophys Prospect* 59: 1144–1154. https://doi.org/10.1111/j.1365-2478.2011.00996.x
43. Dell'Aversana P (2024) An introduction to self-aware deep learning for medical imaging and diagnosis. *Explor Digit Health Technol* 2: 218–234. https://doi.org/10.37349/edht.2024.00023
44. Dell'Aversana P (2024) Enhancing deep learning and computer image analysis in petrography through artificial self-awareness mechanisms. *Minerals* 14: 247. https://doi.org/10.3390/min14030247